Int. J. Rock Mech. Min. Sci. & Geomech. Abstr. Vol. 28, No. 5, pp. 451–456, 1991
Printed in Great Britain.

0148-9062/91 $3.00 + 0.00

Technical Note

A Seismic Velocity-confining Pressure Relation, With Applications

W. W. WEPFER†
N. I. CHRISTENSEN†

INTRODUCTION

In a rock specimen, the constituent minerals and microcracks dictate the sample's response to stress. This behaviour is reflected in the compressional and shear velocities measured as a function of confining pressure in the laboratory, and thus laboratory velocities have been employed to solve important geologic problems. To further this usage, an empirical equation relating velocity to confining pressure is proposed. This equation is used to curve-fit V_p and V_s data for a range of samples and is shown to give excellent results with well-constrained parameters. Expressing a complete V–P data set is reduced to reporting four constants, since data interpolation and extrapolation are accurately performed using this equation. Once the data are curve-fit, pressure derivatives, velocity anisotropies and elastic constants as functions of pressure are simply determined.

A VELOCITY-CONFINING PRESSURE EQUATION

Compressional velocities measured as a function of confining pressure for a Connecticut gneiss are shown in Fig. 1. Velocities were determined using the pulse transmission method of Birch [1] and described in detail by Christensen [2]. The effect of pressure is large below 200 MPa when cracks are being closed under increasing pressure and re-opened when the pressure is decreased [3]. Velocity hysteresis is clearly evident in this region, and this behaviour is generally ascribed to cracks being more easily closed than re-opened. At high pressures, where the influence of cracks is greatly diminished, the slope is small. A transition between a steep and shallow slope usually occurs between 60 and 200 MPa, and this is called the knee region.

The proposed empirical formula is:

$$V(P) = A(P/100\ \text{MPa})^a + B(1 - e^{-bP}), \qquad (1)$$

where P is the confining pressure in MPa, V is the velocity (V_p or V_s) and A, a, B and b are four adjustable parameters. This equation was obtained solely from mathematical considerations (i.e. the shape of each function). Figure 2 shows the effect of varying each model parameter. The solid line is the curve generated using typical values for each of the four parameters: $A = 5$ km/sec, $a = 0.025$, $B = 0.60$ km/sec, $b = 0.025$/

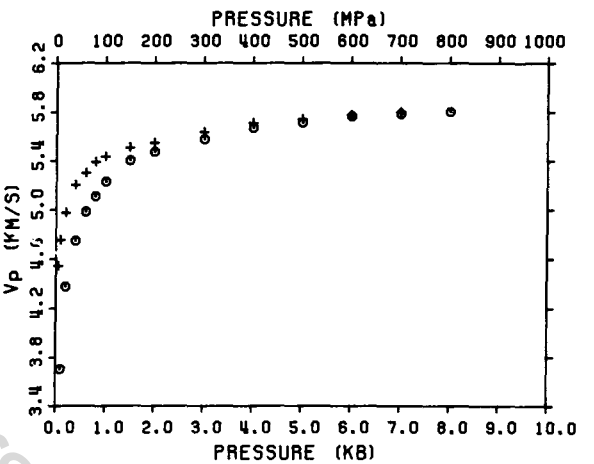

Fig. 1. V_p-Confining pressure data for a Connecticut gneiss. In this and all subsequent figures, the circles and pulses are velocities measured while the pressure was being increased and decreased, respectively. Crack closure governs velocities below 200 MPa, and velocity hysteresis is also evident in this region.

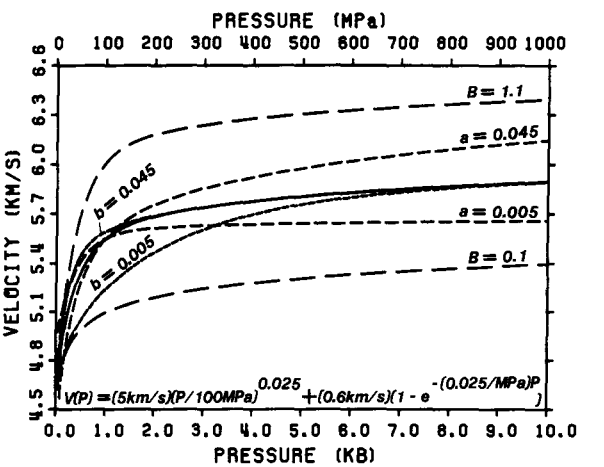

Fig. 2. Parametric analysis of equation (1). The solid curve is given by the equation and represents the following typical values: $A = 5$ km/sec, $a = 0.025$, $B = 0.6$ km/sec, $b = 0.025$/MPa. B, b and a are individually varied as indicated while leaving the others unchanged.

†Department of Earth and Atmospheric Sciences, Purdue Rock Physics Laboratory, Purdue University, West Lafayette, IN 47907, U.S.A.

MPa. While the other three are held constant, a, B and b are individually raised and lowered to their typical maximum and minimum values to produce the six dashed curves. A is not varied because it is primarily a "DC offset." Inspection of this plot shows in which pressure region each variable dominates. The parameter a controls the high-pressure slope (when b is not too small), B determines the magnitude of the velocity increase between 0 and 200 MPa and b defines the shape of the knee.

Examples of the success obtained using equation (1) are given in Fig. 3, and the propagation directions, parameter values, estimated standard deviations, sum of squared residuals (SSR), total number of data points, r.m.s. error and calculated slopes are given in Table 1. Figure 3 provides support of the ability of equation (1) to fit a variety of data, both V_p and V_s; in fact, over 6000 data sets from a range of rock types have been successfully curve-fit using this equation. The four variables are well constrained, with uncertainties in the range of 1% for A, 5–10% for a and 5–25% for B and b (determined from the covariance matrix). Some of the data were curve-fit using a reduced form of equation (1), $V(P) = A(P/100\ \text{MPa})^a$, and these are listed in Table 1.

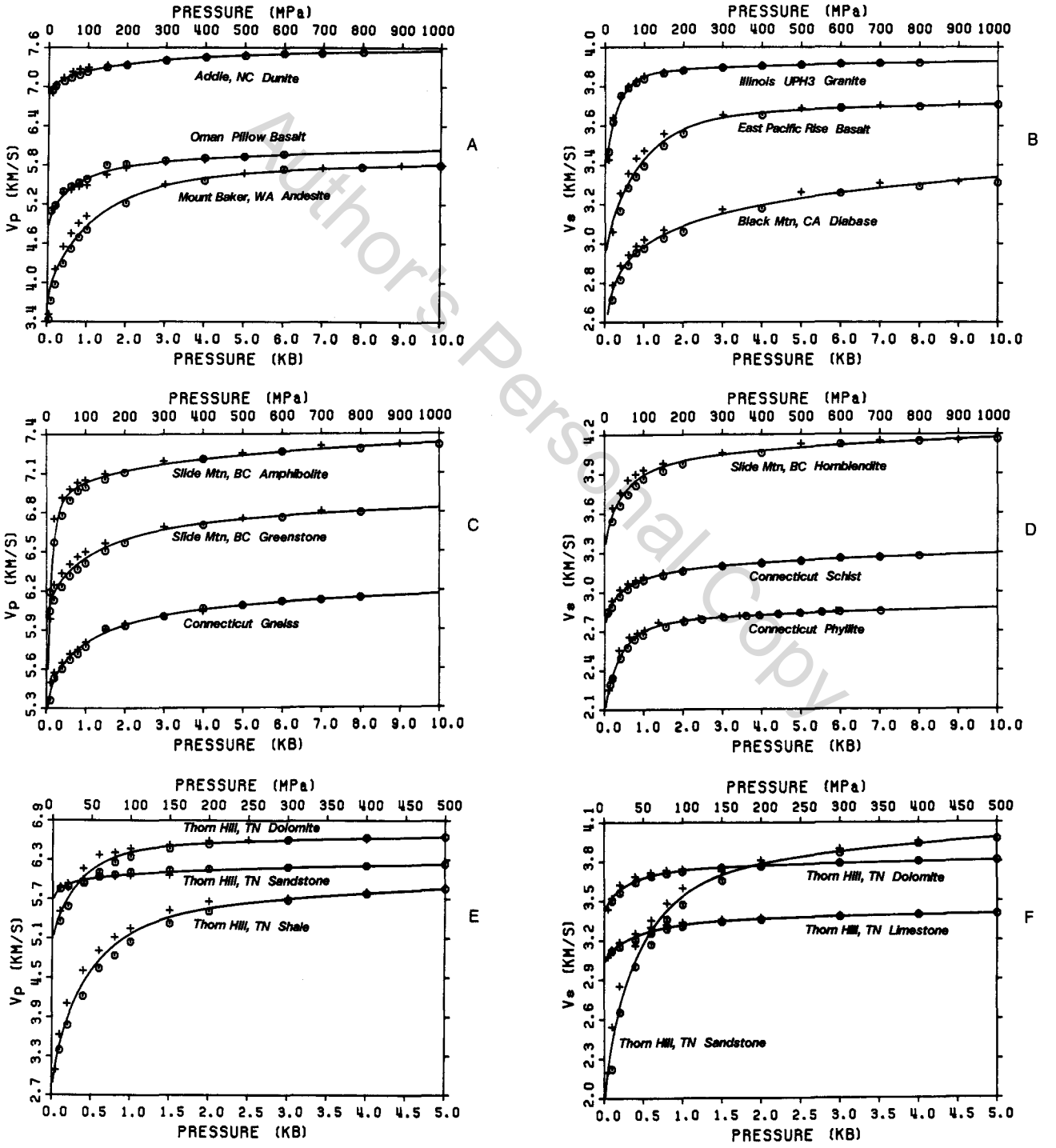

Fig. 3. Equation (1) curve fits various rocks: (A) igneous V_p; (B) igneous V_s; (C) metamorphic V_p; (D) metamorphic V_s; (E) sedimentary V_p; (F) sedimentary V_s.

Table 1. Curve-fit parameters and estimated standard deviations, sum of squared data residual (SSR) in (km/sec)^2, number of data points (n), r.m.s. error in ±km/sec, and calculated slopes for all curved fits. For foliated samples, the Z direction is perpendicular to the foliation, Y is parallel to foliation and lineation, and X is parallel to foliation and perpendicular to lineation. $[Z]$ (Y) indicates propagation in the Z direction and particle motion in the Y direction

Figure No. and sample	A (km/sec)	a	B (km/sec)	b (1/MPa)	SSR	n	r.m.s. Error	dV/dP (km/sec/GPa) 20 MPa	100 MPa	500 MPa
3A, Igneous, V_p										
Dunite	7.16 ± 0.02	0.012 ± 0.002	0.21 ± 0.04	0.0054 ± 0.0007	0.023	27	0.03	5.0	1.48	0.24
Pillow basalt	5.29 ± 0.03	0.026 ± 0.002	0.42 ± 0.04	0.013 ± 0.001	0.041	22	0.05	10.9	2.86	0.29
Andesite	4.21 ± 0.02	0.035 ± 0.001	1.25 ± 0.03	0.0075 ± 0.0002	0.483	22	0.16	15.0	5.89	0.54
3B, Igneous, V_s										
Granite	3.45 ± 0.05	0.0073 ± 0.0009	0.42 ± 0.05	0.032 ± 0.004	0.010	27	0.02	8.3	0.81	0.05
Basalt	3.06 ± 0.03	0.012 ± 0.001	0.56 ± 0.03	0.0107 ± 0.0007	0.021	20	0.04	6.6	2.42	0.10
Diabase	2.988 ± 0.005	0.048 ± 0.001	—	—	0.014	21	0.03	6.7	1.79	0.31
3C, Metamorphic, V_p										
Amphibolite	5.57 ± 0.06	0.0231 ± 0.0008	1.46 ± 0.06	0.087 ± 0.004	0.079	23	0.06	28.4	1.31	0.27
Greenstone	6.31 ± 0.02	0.016 ± 0.002	0.28 ± 0.04	0.0069 ± 0.0009	0.031	20	0.04	6.7	2.00	0.27
Gneiss	5.66 ± 0.02	0.020 ± 0.001	0.24 ± 0.03	0.008 ± 0.001	0.019	27	0.03	7.2	2.01	0.27
3D, Metamorphic, V_p										
Hornblendite	3.67 ± 0.03	0.027 ± 0.002	0.27 ± 0.04	0.018 ± 0.003	0.027	21	0.04	8.2	1.80	0.21
Schist	3.00 ± 0.03	0.025 ± 0.001	0.12 ± 0.03	0.018 ± 0.004	0.005	27	0.02	5.0	1.10	0.15
Phyllite	2.26 ± 0.04	0.025 ± 0.001	0.49 ± 0.04	0.024 ± 0.002	0.011	33	0.02	9.9	1.62	0.12
3E, Sedimentary, V_p										
Dolomite	5.44 ± 0.05	0.017 ± 0.001	1.05 ± 0.05	0.025 ± 0.001	0.139	21	0.09	20.5	3.04	0.19
Shale	6.074 ± 0.005	0.0159 ± 0.0007	—	—	0.009	18	0.02	4.7	0.96	0.20
Sandstone	3.76 ± 0.04	0.072 ± 0.002	1.64 ± 0.04	0.0198 ± 0.0006	0.303	22	0.13	33.9	7.20	0.61
3F, Sedimentary, V_s										
Sandstone	2.61 ± 0.04	0.071 ± 0.002	1.06 ± 0.04	0.0210 ± 0.0009	0.134	22	0.09	22.8	4.57	0.41
Dolomite	3.58 ± 0.04	0.011 ± 0.001	0.16 ± 0.04	0.028 ± 0.005	0.007	22	0.02	4.6	0.68	0.08
Limestone	3.17 ± 0.03	0.011 ± 0.002	0.17 ± 0.04	0.019 ± 0.004	0.004	22	0.02	4.0	0.84	0.07
4 Metagreywacke										
1st run	5.04 ± 0.05	0.0267 ± 0.0007	0.91 ± 0.05	0.036 ± 0.002	0.731	33	0.16	22.4	2.25	0.28
2nd run	5.41 ± 0.05	0.0240 ± 0.0007	0.55 ± 0.05	0.037 ± 0.004	0.095	31	0.06	16.1	1.81	0.27
6 Phyllite										
$[Z]$	3.877 ± 0.003	0.1240 ± 0.0005	—	—	0.140	33	0.07	19.7	4.81	1.17
$[Y]$	6.890 ± 0.004	0.0224 ± 0.0003	—	—	0.053	32	0.04	7.5	1.55	0.32
$[X]$	5.87 ± 0.02	0.026 ± 0.001	0.55 ± 0.02	0.0103 ± 0.0006	0.113	34	0.06	11.9	3.54	0.35
7 Gneiss										
$[Z]$	4.08 ± 0.03	0.047 ± 0.001	1.46 ± 0.03	0.0127 ± 0.0003	0.384	35	0.11	23.4	7.15	0.45
$[Y]$	5.25 ± 0.02	0.037 ± 0.001	0.86 ± 0.03	0.0101 ± 0.0004	0.267	28	0.11	16.2	5.09	0.47
$[X]$	5.03 ± 0.02	0.016 ± 0.002	1.09 ± 0.03	0.0080 ± 0.0002	0.227	28	0.10	11.3	4.73	0.32
$[Z](Y)$	2.71 ± 0.03	0.034 ± 0.002	0.84 ± 0.03	0.0168 ± 0.0008	0.016	30	0.03	14.5	3.57	0.20
$[Y](X)$	3.17 ± 0.02	0.021 ± 0.002	0.59 ± 0.03	0.0119 ± 0.0007	0.033	32	0.04	8.8	2.80	0.16
$[Y](Z)$	2.56 ± 0.03	0.023 ± 0.002	0.93 ± 0.03	0.0140 ± 0.0006	0.051	30	0.04	12.7	3.79	0.13
V_p averaged	4.81 ± 0.02	0.0337 ± 0.0006	1.10 ± 0.02	0.0103 ± 0.0003	0.000	46	0.00	16.9	5.67	0.41
V_s averaged	2.81 ± 0.03	0.0267 ± 0.0008	0.78 ± 0.03	0.0144 ± 0.0006	0.000	46	0.00	12.0	3.41	0.16
10 Granulite										
Pts to 1000 MPa	5.69 ± 0.04	0.0251 ± 0.0006	0.74 ± 0.04	0.012 ± 0.001	0.244	21	0.12	16.6	3.53	0.30
Pts to 600 MPa	5.66 ± 0.04	0.020 ± 0.002	0.81 ± 0.04	0.017 ± 0.001	0.285	21	0.13	15.2	3.69	0.24

All points were included in the curve-fits, thereby roughly bisecting the hysteresis section. This is equivalent to the bisection used by Brown and Scholz [4] on their stress–strain hysteresis loops of Birch [2] for velocity data. Support for this approach is provided by further analysis of velocity behaviour below 200 MPa. The effect of previous pressurizations on the subsequently observed velocities is great for the first few runs of a sample, with the largest change occurring between the first and second runs. This is illustrated in Fig. 4 for an Alaskan metagreywacke. Five minutes transpired between the two runs and the sample assembly was left undisturbed in the pressure vessel during this time. Clearly the up-going pressure velocities have significantly increased from the first to the second run, while the down-going pressure velocities are virtually coincident for the two runs. The reduced hysteresis of the second run reflects the reduced influence of cracks, a behaviour that is more representative of rocks at *in situ* pressures and temperatures (the cause of hysteresis are discussed more fully below). In particular, the up-going velocities of the second run are probably the best estimate of the rock's behaviour at depth. Bisecting the hysteresis region with a curve-fit of all of the first run data is therefore appropriate because it closely approximates the up-going velocities of the second run, and obviously this avoids the need for two or more pressurizations.

ADDITIONAL APPLICATIONS

Pressure derivatives and pore pressure

Since the data are expressed analytically using equation (1), pressure derivatives of velocities are simple to calculate. Table 1 lists some of these at selected

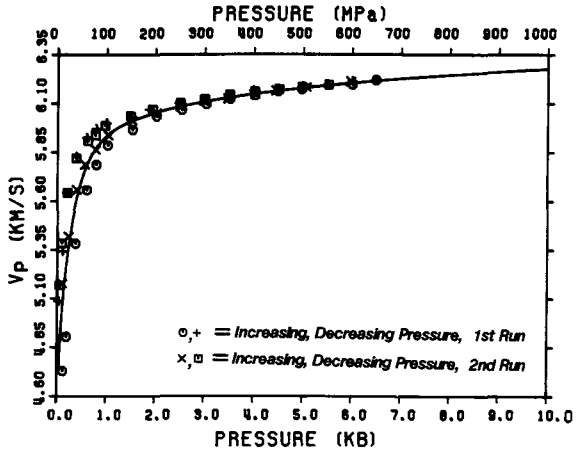

Fig. 4. V_p Data for an Alaskan metagreywacke pressurized ("run") twice. The curve fit is for the first run, although it coincides with the up-going values of the second run. Hysteresis decreases from the first to the second run because of irreversible crack damage. Note the overlap between the down-going pressure velocities of both runs.

pressures. The derivatives at high pressures can be used in the critical geothermal gradient equation:

$$\frac{dV}{dz} = \left(\frac{\partial V}{\partial P}\right)_T \frac{dP}{dz} + \left(\frac{\partial V}{\partial T}\right)_P \frac{dT}{dz}$$

[5] or in the Adams–Williamson equation [6]. Derivatives are also used in the determination of the parameter n from the effective pressure relation:

$$P_e = P_c - nP_p$$

[7], where P_e is the effective pressure, P_c is the confining pressure and P_p is the pore pressure; n is less than or equal to one. The value of n is determined using the equation:

$$n = 1 - (\partial V/\partial P_p)_{P_d}/(\partial V/\partial P_d)_{P_p}$$

[8] where P_d is the differential pressure, $P_d = P_c - P_p$. Figure 5 gives the velocities for a Juan de Fuca Ridge basalt at varying pore pressure. The slope at constant differential pressure is easily determined using standard linear regression. By substituting P_d for P_c, equation (1)

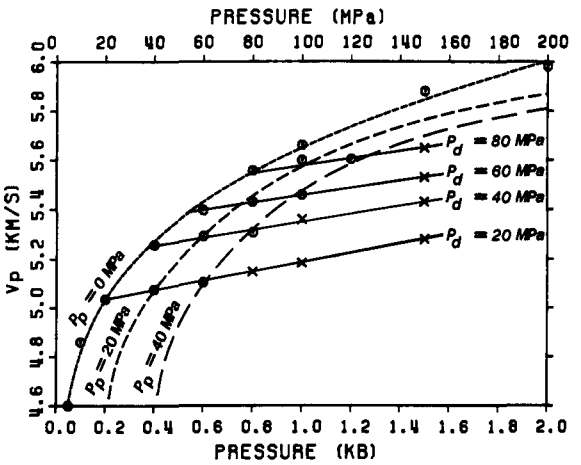

Fig. 5. V_p Pore pressure (P_p) data from a Juan de Fuca Ridge basalt. Dashed lines are equation (1) constant P_p curve fits, and constant differential pressure (P_p) linear regression fits are solid. The P_p and P_d slopes give the parameter n from the effective pressure relation. The data are from Christensen [8].

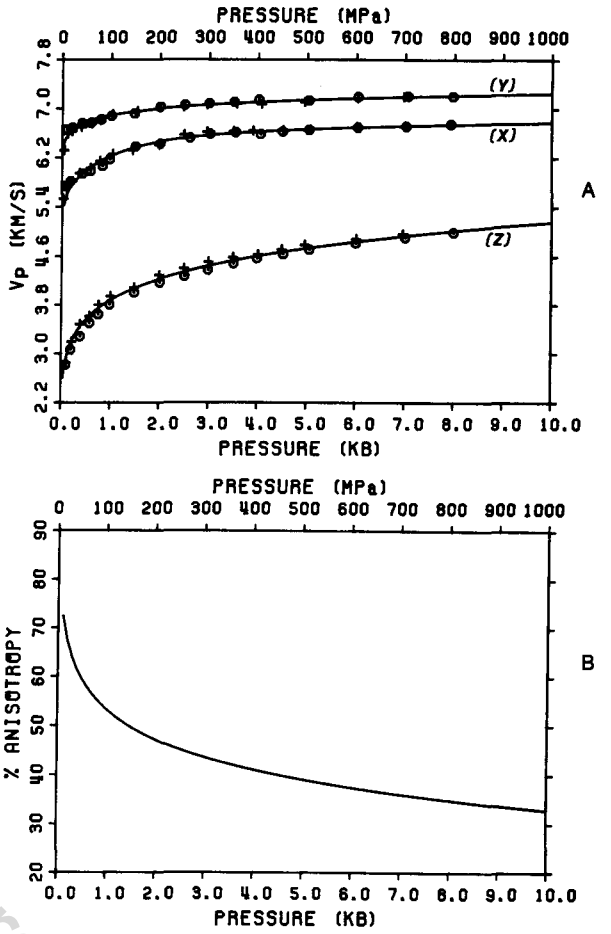

Fig. 6. (A) V_p Data for an anisotropic phyllite from North Carolina (see Table 1 for propagation descriptions). (B) V_p Anisotropy as a function of pressure calculated from the three curve fits. The decrease in anisotropy with pressure is due to crack closure.

is generalized to include velocities determined at constant pore pressure:

$$V(P_d) = A(P_d/100\ \text{MPa})^a + B(1 - e^{-bP_d}).$$

Three curve-fits using this formula are indicated by solid lines in Fig. 5. Derivatives of these curves give the otherwise difficult to obtain slopes at constant pore pressures.

Velocity anisotropy

Figure 6 shows three compressional velocities measured in orthogonal directions on a phyllite. The equation (1) curve-fits enable a straightforward calculation of velocity anisotropy as a function of pressure using:

$$\%\ \text{anisotropy} = \left(\frac{V_{max} - V_{min}}{V_{avg}}\right) \times 100,$$

where V_{max}, V_{min} and V_{avg} are the maximum, minimum and average velocities, respectively, at a given pressure. The anisotropy as a function of pressure for the phyllite is also shown in Fig. 6. Clearly the V_p anisotropy decreases with increasing confining pressure. This is due to crack closure, the same conclusion drawn by Brace [9] for compressibility anisotropy and by Wissler and Simmons [10] for strain anisotropy.

Elastic constants

Calculating equivalent isotropic elastic constants of rocks from velocities and densities is likewise a simple procedure. As shown by Christensen and Ramananantoandro [11], the isotropic elastic constants of an anisotropic rock are closely approximated by those derived using the average of the compressional and shear velocities measured in the three principal directions. This is the meaning of the term "equivalent" isotropic elastic constants. Figure 7A shows the V_p and V_s curve-fits obtained for a Connecticut gneiss. The dashed lines are the average V_p and V_s curves generated from the three curve-fits for each wave type, and these curves are used to determine the isotropic elastic constants. The calculated Poisson's ratios and shear moduli as functions of confining pressure are shown in Fig. 7B. The dip in Poisson's ratio at 100 MPa is an intriguing feature

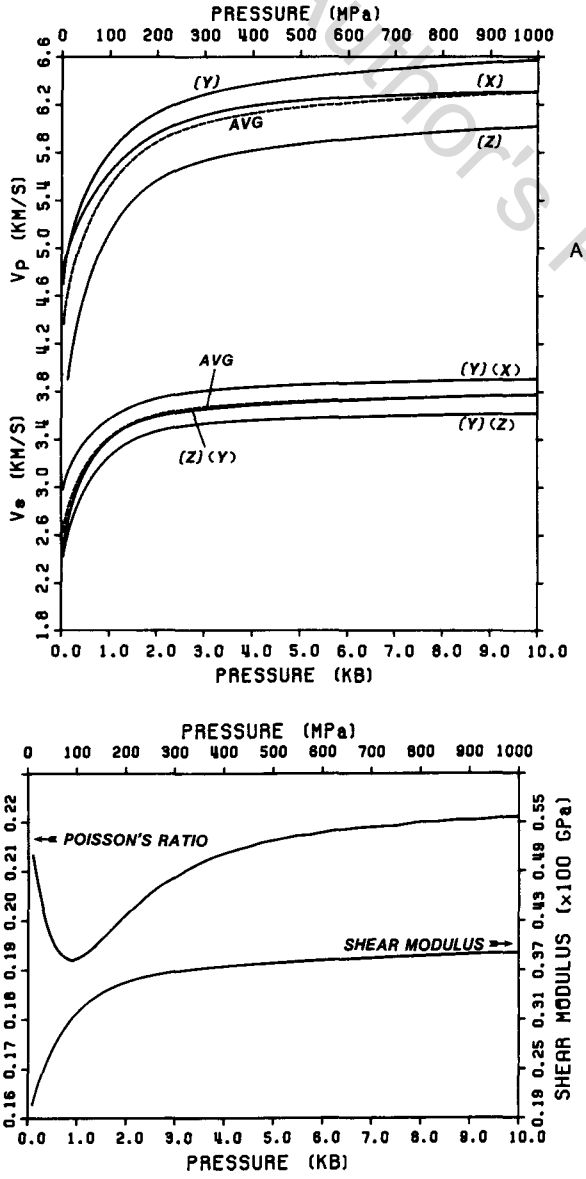

Fig. 7. (A) Equation (1) curve-fits (solid lines) and average V_p and V_s curves (dashed) for a Connecticut gneiss. Table 1 gives propagation descriptions. (B) Equivalent isotropic elastic constants determined from the average curves in (A). Note the dip in Poisson's ratio at 100 MPa, a feature which may be crack related.

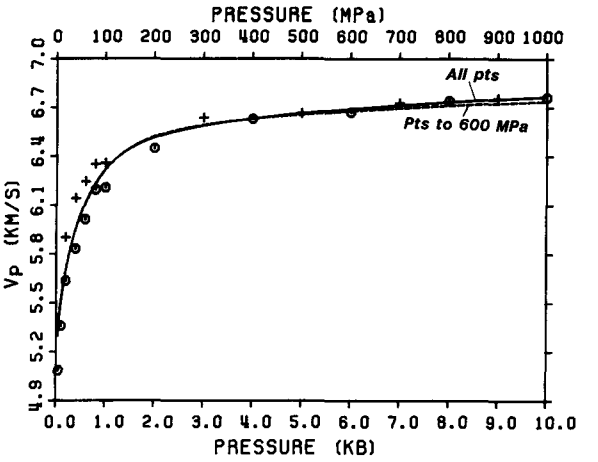

Fig. 8. New York granulite V_p data. The solid curve was calculated using all of the data, the dashed curve used only the points to 600 MPa. The high-pressure velocities extrapolated by the dashed curve are well within the experimental error of the measured velocities.

observed in more than a few samples. Its significance is uncertain, but it may be crack related (a different response of V_s to crack closure than V_p). curve fits using equation (1) could also be used to calculate more complicated elastic constants, e.g. if the five appropriate velocity–pressure data sets were available for a transversely isotropic sample, the five elastic constants could be calculated as functions of pressure.

Interpolation and extrapolation

Interpolation and extrapolation of velocities is a significant advantage of employing a velocity–pressure curve-fit. Adequate interpolation using equation (1) is clear from all of the curve-fits given above. These plots also show the smoothing of data variations by curve-fitting. Accurate data extrapolation using equation (1) is illustrated in Fig. 8. The solid curve was determined using all of the data points. Only the velocities at pressures to 600 MPa were used to calculate the dashed curve, yet this adequately approximates the velocities at higher pressures. At 1000 MPa, the difference between the dashed curve and the measured velocity is less than 0.5%, which is well within the experimental error of 1%. Thus equation (1) can be employed to extrapolate velocities at higher pressures, but only when enough high-pressure data are available to constrain the curve.

Velocity hysteresis

Finally, velocity hysteresis can be quantitatively evaluated using equation (1). The sum of squared residuals (SSR) determined with each curve-fit primarily reflects velocity variations at pressures below 200 MPa, thereby giving an indication of the amount of hysteresis. Using the data given in Fig. 4, the SSR for the first run is 0.731 $(km/sec)^2$ while that for the second is only 0.095 $(km/sec)^2$. The SSR therefore states numerically what is visually obvious from Fig. 4, namely that the velocity hysteresis decreases significantly from the first to the second run.

CONCLUSIONS

The velocity–confining pressure relation:

$$V(P) = A(P/100\ \text{MPa})^a + B(1 - e^{-bP}),$$

is employed to curve-fit laboratory V_p and V_s data from a variety of rocks. The four adjustable parameters, A, a, B and b are well-constrained and robust to poor quality data. Velocity interpolation and extrapolation are quickly and accurately performed, and thus the four parameters from the equation briefly render a complete description of a velocity–pressure data set. Brevity is particularly important when one considers the quantity of data generated for most studies with modern laboratory equipment.

Once the data are expressed analytically, a number of calculations are simplified. Velocity pressure derivatives, such as those required in the critical geothermal gradient equation or for the effective pore pressure relation, are easily calculated using the V–P equation. Determining the velocity anisotropy as a function of pressure for a sample is also straightforward. The decrease in anisotropy with increasing pressure is attributed to microcrack closure and may reflect any preferred crack orientation. Elastic constants are likewise simple to determine. For some samples, a drop in Poisson's ratio is found at about 100 MPa. Its origin is unknown, but it may be crack related.

The response of velocities to confining pressure can be qualitatively described in terms of crack closure based on the SEM work of Batzle *et al.* [13]. At pressures below 200 MPa, the closure is characterized by the crack wall separation and topography. Above this pressure, the crack wall roughness alone dictates further closure. Velocity hysteresis is caused by the cracks sticking shut when subjected to high pressures. The parameters in the velocity–pressure equation may be related to this crack behaviour. If so, B is associated with the crack wall separation at low pressures (below 200 MPa), b with the crack wall mismatch at low pressures, and a with the crack wall topography at pressures above 200 MPa. The parameter A is related to the zero pressure velocity.

Acknowledgements—Our gratitude to the many who have acquired data for N. I. Christensen over the past 25 years, with particular thanks to D. Kingma, C. Wilcox and D. Szymanski. The comments proffered by R. L. Nowack, as well as the course which prompted this work, are greatly appreciated. This research was supported by the Office of Naval Research under Contracts N-00014-84-K-0207 and N-00014-89-J-1209 (N. I. Christensen) and by a Purdue David Ross fellowship (W. W. Wepfer).

Accepted for publication 5 February 1991.

REFERENCES

1. Birch F. The velocity of compressional waves in rocks to 10 kilobars, Part 1. *J. Geophys. Res.* **65,** 1083–1102 (1960).
2. Christensen N. I. Measurements of dynamic properties of rock at elevated pressures and temperatures. In *Measurement of Rock Properties at Elevated Pressures and Temperatures* (Edited by H. J. Pincus and E. R. Hoskins), pp. 93–107. American Society for Testing and Materials, Philadelphia, ASTM STP 869 (1985).
3. Birch F. The velocity of compressional waves in rocks to 10 kilobars, Part 2. *J. Geophys. Res.* **66,** 2199–2224 (1961).
4. Brown S. R. and Scholz C. H. The closure of random elastic surfaces in contact. *J. Geophys. Res.* **90,** 5531–5545 (1985a).
5. Christensen N. I. Compressional wave velocities in rocks at high temperatures and pressures, critical thermal gradients, and crustal low-velocity zones. *J. Geophys. Res.* **84,** 6849–6857 (1979).
6. Adams L. H. and Williamson E. D. The compressibility of minerals and rocks at high pressures. *J. Franklin Inst.* **195,** 475–529 (1923).
7. Todd T. and Simmons G. Effect of pore pressure on the velocity of compressional waves in low-porosity rocks. *J. Geophys. Res.* **77,** 3731–3743 (1972).
8. Christensen N. I. Pore pressure and oceanic crustal seismic structure. *Geophys. J. R. Astr. Soc.* **79,** 411–424 (1984).
9. Brace W. F. Some new measurements of linear compressibility of rocks. *J. Geophys. Res.* **70,** 391–398 (1965).
10. Wissler T. M. and Simmons G. The physical properties of a set of sandstones—Part II: permanent and elastic strains during hydrostatic compression to 200 MPa. *Int. J. Rock Mech. Min. Sci. & Geomech. Abstr.* **22,** 393–406 (1985).
11. Christensen N. I. and Ramananantoandro R. Elastic moduli and anisotropy of dunite to 10 kilobars. *J. Geophys. Res.* **76,** 4003–4010 (1971).
12. Sprunt E. and Brace W. F. Direct observation of microcavities in crystalline rocks. *Int. J. Rock Mech. Min. Sci. & Geomech. Abstr.* **11,** 139–150 (1974).
13. Batzle M. L., Simmons G. and Siegfried R. W. Microcrack closure in rocks under stress: Part I, direct observation. *J. Geophys. Res.* **85,** 7072–7090 (1980).